sustainability

MDPI

Article

Spatiotemporal Analysis of Forest Fires in China from 2012 to 2021 Based on Visible Infrared Imaging Radiometer Suite (VIIRS) Active Fires

Bing Dong, Hongwei Li, Jian Xu, Chaolin Han and Shan Zhao *

School of Geoscience and Technology, Zhengzhou University, Zhengzhou 450001, China; dongbingling@gs.zzu.edu.cn (B.D.); lhw29691518@zzu.edu.cn (H.L.); xj0102@gs.zzu.edu.cn (J.X.); hhcl@gs.zzu.edu.cn (C.H.)

* Correspondence: zhaoshan4geo@zzu.edu.cn; Tel.: +86-137-0087-5423

Abstract: Forest fire regimes are changing as a function of increasing global weather extremes, socioeconomic development, and land use change. It is appropriate to use long-term time series satellite observations to better understand forest fire regimes. However, many studies that have analyzed the spatiotemporal characteristics of forest fires based on fire frequency have been inadequate. In this study, a set of metrics was derived from the VIIRS active fire data in China, from 2012 to 2021, through spatial extraction, spatiotemporal clustering, and spread reconstruction to obtain the frequency of forest fire spots (FFS), the frequency of forest fire events (FFE), the frequency of large forest fire events (LFFE), duration, burned area, and spread rate; these metrics were compared to explore the characteristics of forest fires at different spatiotemporal scales. The experimental results include 72.41×10^4 forest fire spots, 7728 forest fire events, 1118 large forest fire events, and a burned area of 58.4×10^4 ha. Forest fires present a significant spatiotemporal aggregation, with the most FFS and FFE in the Southern Region and the most severe LFFE and burned area in the Southwest Region. The FFS, FFE, and LFFE show a general decreasing trend on an annual scale, with occasional minor rebounds. However, the burned area had substantial rebounds in 2020. The high incidence of forest fires was concentrated from March to May. Additionally, 74.7% of the forest fire events had a duration of less than 5 days, while 25.3% of the forest fire events lasted more than 5 days. This helps us to understand the characteristics of more serious or higher risk forest fires. This study can provide more perspectives for exploring the characteristics of forest fires, and more data underpinning for forest fire prevention and management. This will contribute towards reasonable forest protection policies and a sustainable environment.

Keywords: Visible Infrared Imaging Radiometer Suite (VIIRS); forest fire; spatiotemporal characteristics; spatiotemporal clustering; spread reconstruction; China

Citation: Dong, B.; Li, H.; Xu, J.; Han, C.; Zhao, S. Spatiotemporal Analysis of Forest Fires in China from 2012 to 2021 Based on Visible Infrared Imaging Radiometer Suite (VIIRS) Active Fires. *Sustainability* **2023**, *15*, 9532. https://doi.org/10.3390/su15129532

Academic Editor: Antonio Miguel Martínez-Graña

Received: 17 May 2023
Revised: 11 June 2023
Accepted: 12 June 2023
Published: 14 June 2023

1. Introduction

Forest fires are a major global concern, as they burn millions of hectares of forests every year [1]. These fires have caused extensive damage to forest resources by directly reducing forest area and seriously damaging forest structure and the environment [2], resulting in imbalances in forest ecosystems [3], and even threatening human life and property if serious [4,5]. In recent years, with socioeconomic development and land use changes, anthropogenic-driven fire regimes have become increasingly important [6,7]. Moreover, with a warmer climate, the frequency and burned area of fires are expected to increase globally in the future [8–10], and the duration of the fire season will be extended [10,11]. As a result, fire regimes are changing [12–14].

The use of remote sensing data to study forest fire regimes has been shown to be very effective [15–17], since it allows easy access to global, consistent, and long-term historical

forest fire data There have been many studies that have quantitatively described and analyzed the spatial and temporal distribution of global fires [18–21] or specific regions [22,23]. Currently, the commonly used remote sensing data are MODIS Collection 6 [24] (Moderate Resolution Imaging Spectroradiometer C6, with a spatial resolution of 1 km, temporal resolution of four times per day, first released in 2001) and VIIRS V1 [25] (Visible Infrared Imaging Radiometer Suite V1, with a spatial resolution of 375 m, temporal resolution of two times per day, first released in 20 January 2012), which provide information such as the location, time, and radiation energy [26,27]. In this study, we chose VIIRS because it provides active fire data with a higher spatial resolution, can monitor forest fires with more precise locations, and can observe forest fires at a smaller scale.

China is a country with a high incidence and vulnerability to forest fires [15]. According to the 9th China Forest Inventory, China's forest cover is only 22.96% and it is unevenly distributed, which, together with the complex climate and terrain, leads to differences in forest fire characteristics across the country. Therefore, there is a need to investigate the regional variations and temporal changes of forest fires in China. Currently, many scholars have conducted research on the spatiotemporal characteristics of fires in China [15,28,29]. The primary sources of active fires in China are cropland fires and forest fires [30]. Cropland fires have predominantly occurred in the agricultural regions of Northeastern, Northern, and Northwestern China [31,32], and forest fires have frequently been observed in the forested regions of Northeastern, Southwestern, and Southeastern China [33–35]. However, most of these studies have solely focused on the frequency of fire spots, rather than on fire events. Meanwhile, many scholars have also reconstructed fires using various methods to estimate the burned area and spread rate. For instance, Kriging interpolation [36] has been employed to model the daily progress of fires, while Delaunay triangulation [37,38] has been used to construct burned areas. Most of these studies aimed to analyze the development of certain (manually selected) fire events. This study is expected to process remote sensing data, and therefore, derives more comprehensive information on fires, not only in terms of frequency of fire spots, but also in terms of fire events.

In this paper, we use the 10-year VIIRS data (2012–2021) and China's land cover data to extract fire spots within forestlands, to cluster them into fire events, to filter large fire events, and to reconstruct their spread, thus, obtaining the following series of forest fire metrics: the frequency of forest fire spots (FFS), the frequency of forest fire events (FFE), the frequency of large forest fire events (LFFE), duration, burned area, and spread rate. Before analyzing the data, a correlation analysis was conducted to reveal the relationships and usable values among the main metrics. In the formal analysis, first, we aggregated calculations based on the FFS, FFE, LFFE and, burned area at different spatial scales, including the whole country, the five regions, and each province/region, to unveil the spatial distribution of frequency and scale of forest fires in China. Secondly, statistical analyses were carried out for the whole country and the five regions at different time scales, including years and months, to illustrate the spatial and temporal variations in forest fires. In addition, we describe the duration and spread rate of forest fire events. This study attempts to analyze the forest fire spatiotemporal characteristics from multiple perspectives, laying the data foundation for more in-depth research work, such as forest fire risk assessment and fire spread prediction modeling. This study also serves as a reference for conducting forest fire research based on remote sensing data.

2. Materials and Methods

2.1. Study Area

The total land area of China is approximately 9.6×10^6 km^2. The latitude difference between north and south is about 50°, and the terrain and climate are complex and diverse. The north is dry, and the south is relatively wet [39]. The northwest is the main dry area of the country [40]. Precipitation in China gradually decreases from southeast to northwest [41]. The topography in China exhibits a gradient of lower elevation in the east, higher elevation in the west, and mountains covering approximately two-thirds of the

country's land area [42]. These factors have led to spatial and temporal variations in the pattern of forest fires across China.

China's forest area is 220,446,200 ha, with most of it concentrated in the Southwest, Northeast, and Southern Regions. To better reflect the regional variations of forest fires, we divided the study area into five regions: Southwest Region, Northeast Region, Southern Region, Northwest Region, and N-E-China Region. The Southwest Region, including Yunnan Province, Sichuan Province, and Chongqing City, has a total forest area of 43×10^6 ha (19.5% of China's forest area) with forest covering 49.1%. The Northeast Region, including Heilongjiang Province, Jilin Province, and Liaoning Province, has a total forest area of 33.47×10^6 ha (15.2% of China's forest area) with forest covering 42.4%. The Southern Region, which includes 11 provinces including Guangxi, Jiangxi, Guangdong, Fujian, and Zhejiang, has a total forest area of 81.19×10^6 ha (36.8% of China's forest area) with forest covering 45.3%. However, the Northwest and N-E-China Regions have lower forest cover than these regions, with a forest area of 41.75×10^6 ha and 42.02×10^6 ha, respectively. The forest cover in the regions is only 9.7% and 22.3%, highlighting the serious uneven distribution of forest resources in China.

The study area includes the whole of China except the Nansha Islands, Taiwan Province, Hong Kong, and Macao. With the help of land cover data [43], we present the study area in Figure 1, as well as the distribution of forest resources in China and the five geographical regions.

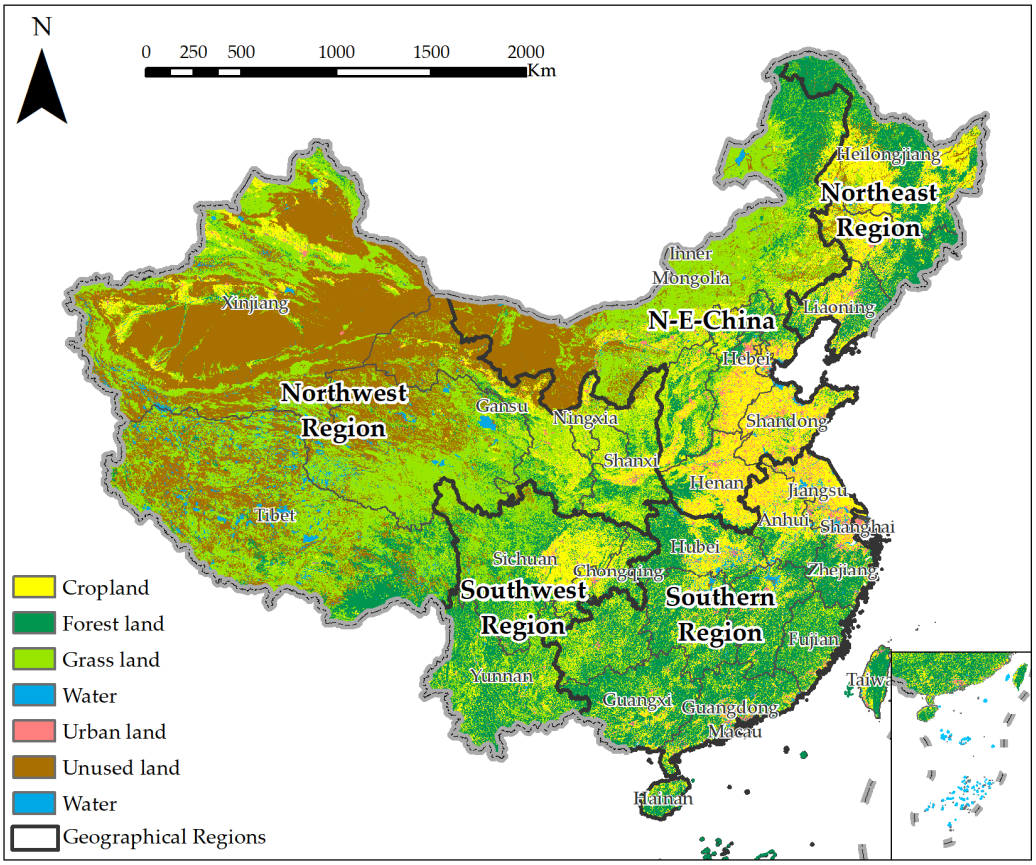

Figure 1. Map of land cover in China in 2020 [43]. The Southwest Region consists of Sichuan Province, Yunnan Province, and Chongqing City; the Northeast Region consists of Heilongjiang, Jilin, and Liaoning Provinces; the South Region consists of 11 provinces, namely Anhui, Jiangsu, Hubei, Hunan, Jiangxi, Zhejiang, Fujian, Guangxi, Guangdong, Hainan, and Guizhou; the Northwest Region consists of 6 provinces/regions, namely Tibet, Xinjiang, Qinghai, Gansu, Ningxia, and Shaanxi; the N-E-China Region consists of 8 of provinces/cities, namely Beijing, Tianjin, Shanghai, Hebei, Henan, Shanxi, Shandong, and Inner Mongolia.

2.2. Study Data

2.2.1. VIIRS Active Fire Data

The VIIRS active fire data used in this paper were obtained through the Fire Information for Resource Management System (https://firms.modaps.eosdis.nasa.gov/download/, accessed on 20 February 2023, in Shapefile format). These data are considered to be near-real-time active fire data and are provided by the National Aeronautics and Space Administration (NASA) and the Food and Agriculture Organization (FAO) of the United Nations. The data have a nominal horizontal resolution of approximately 375 m and provide complete global coverage every 12 h. Since the data have high spatial and temporal resolution and have been widely used in fire research, we chose to use the VIIRS active fire data to analyze the spatial and temporal variations of forest fires in China over the decade 2012–2021. The main focus of our analysis was on fire spot locations, acquisition date, and time information.

2.2.2. Land Cover Data

The land cover data used in this study are the 1 km × 1 km land cover data for 2020 provided by the Institute of Geographical Sciences and Resources of the Chinese Academy of Sciences [43]. The data classify land into 6 categories: cropland, forest land, grassland, water, urban land, and unused land. Since the land cover data change every year, the forest area has gradually increased from 207,687,300 ha in the 8th China Forest Inventory (2009–2013) to 220,446,200 ha in the 9th China Forest Inventory (2014–2018). As a result, the number of fire spots extracted using the 2020 forest area is higher. Nevertheless, for a large number of forest fire spots, the redundant forest fire spots do not substantially affect the characteristics of forest fires.

2.3. Data Processing Methods

To extract forest fire spots, we overlaid the 2012–2021 VIIRS active fire data with the 1 km × 1 km land cover data. Over the 10-year period, there were 5.24×10^6 fire spots in China, but after filtering using the land cover data, the total number of forest fire spots was reduced to 72.41×10^4, representing an overall reduction of 86.2% (including 38.9% for cropland fire spots, 32.4% for urban land fire spots, 8.9% for grassland fire spots, etc.). Most of the subsequent data processing and analysis were conducted based on the remaining forest fire spots, using ArcGIS (version 10.5, a GIS software developed by ESRI) and Python 3.8 tools. Figure 2 depicts the process flowchart for producing data on forest fire spots, forest fire events, and large forest fire events, and the main information contained in them.

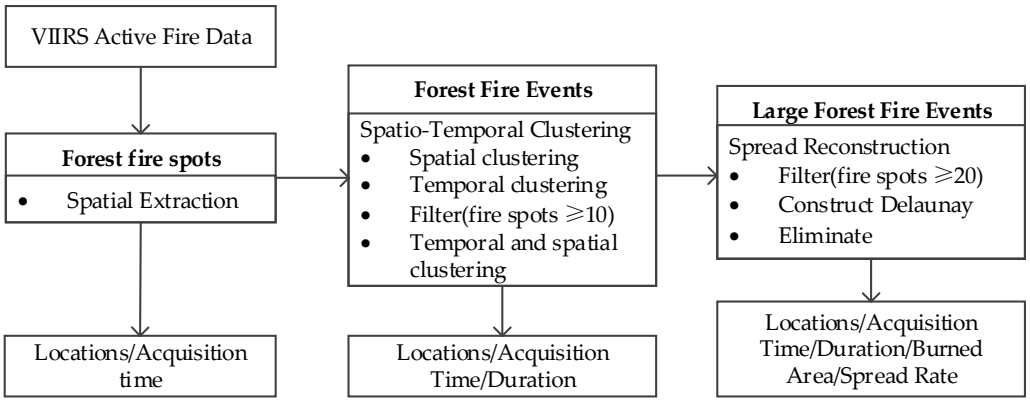

Figure 2. Forest fire data process flowchart.

2.3.1. Method of Spatiotemporal Clustering

Based on the proximity of the location and the time of fire spots in a forest fire event [36], we applied clustering techniques to group discrete fire spots into independent forest fire events using temporal and spatial thresholds. The specific steps involved the

following: (1) clustering in space (threshold of 2 km); (2) clustering in time within each space cluster (threshold of 2 days); (3) filtering out clusters with less than 10 fire spots to exclude sporadic fire spots, smaller fires, or incompletely monitored forest fires; and (4) for the remaining clusters, clustering again in space and time in order to process spots that are close in time but more than 2 km apart in space. Finally, each cluster was identified as a forest fire event.

When choosing thresholds, on the one hand, if the space threshold or time interval is too large, it can group together discrete fires into one event. On the other hand, if the threshold is too small, it can divide a complete fire event into multiple parts. After filtering in Step 3, the remaining forest fire events were at a certain scale with a higher risk, and had greater research value.

Each forest fire event was assigned a unique ID, and its duration was determined by calculating the time difference between the latest and earliest time. This duration indicated how long the fire event lasted. For instance, a duration of 0 signified a fire event that lasted less than 12 h, while a duration of 0.5 days suggested a fire event lasting between 12 h and 1 day. Additionally, forest fire events included information on location, start time, and end time. For example, the forest fire event that occurred in Sichuan Province in 2020 (Figure 3) started at 2:00 on 26 December 2020 and ended at 14:00 on 7 January 2021, lasted 12.5 days, and involved 1477 forest fire spots.

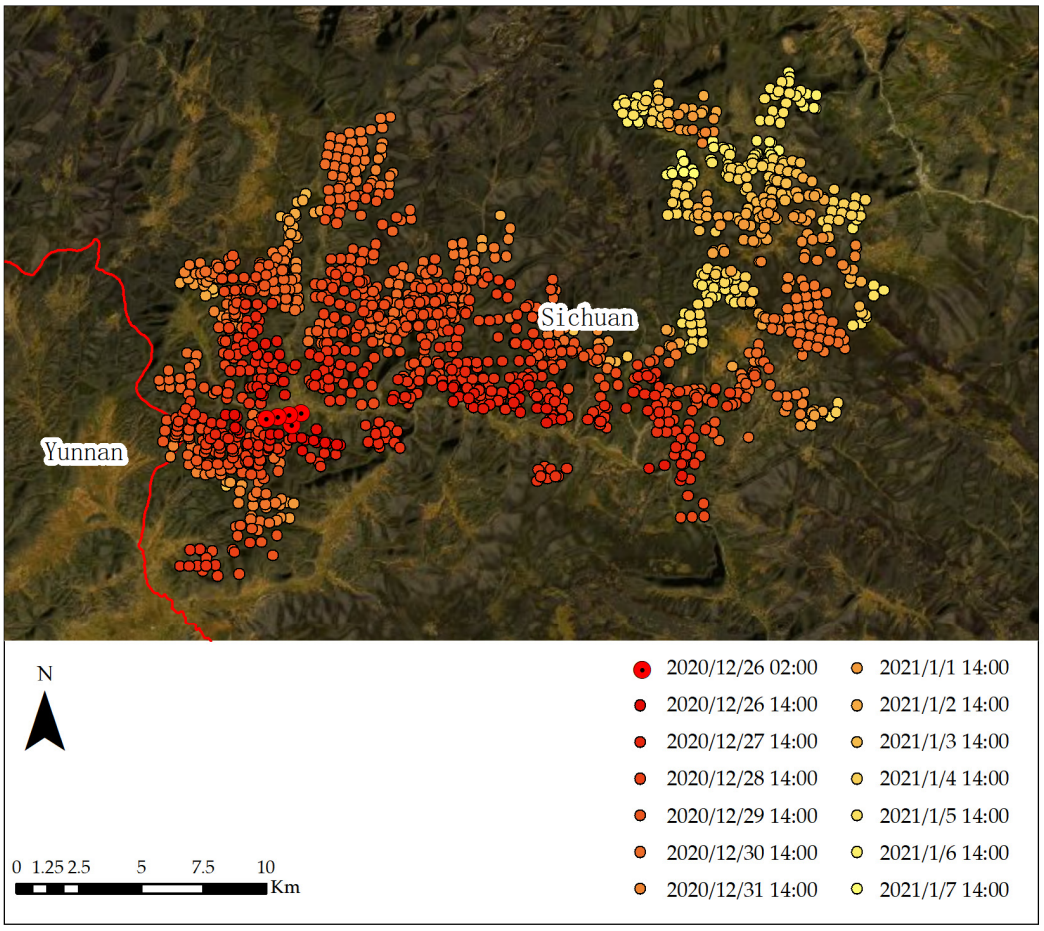

Figure 3. An example of the results of a spatiotemporal clustering: The forest fire that occurred in Sichuan Province in 2020.

2.3.2. Method of Spread Reconstruction

Forest fire spread reconstruction is a modeling approach that aims to recreate the development of a forest fire based on a series of fire spots. In real-life scenarios, medium to large forest fire events occur less frequently but are more destructive, last longer, and

occupy larger areas. To more accurately reconstruct the burned area and represent the spread of forest fires, forest fire events with more than 20 (≥20) fire spots that lasted longer than 2 days (≥2 d) were selected, as they had more complete monitoring information. The specific steps for forest fire spread reconstruction included: (1) constructing a Delaunay triangulation for each forest fire event with control sides no longer than 2 km; (2) removing larger triangles (area > 500 ha) to eliminate areas with low fire spot density and to address possible unburned holes within the burned area; (3) merging each forest fire Delaunay triangulation of an event, representing the burned area of forest fire; and (4) constructing the spread vector of a forest fire, from the earliest monitored fire spot (at time t) to the furthest spot (at time s (s > t)). The vector used to track the spread of a forest fire, and its length divided by the time difference (s – t) represents the average spread rate of the forest fire event. This part of the forest fire selection is for forest fire events that last longer than 2 days and have a cluster of more than 20 fire spots, and therefore can be considered to be large-scale forest fires.

Here, since the time difference between the origin spot and the furthest spot is at least 12 h (reason of the temporal resolution of VIIRS), it is difficult for a forest fire to maintain a uniform spread rate over such a long period of time. Therefore, the spread rate only represents the average spread rate, which may be smaller due to the lag in monitoring. Of course, there may be multiple spots in the earliest monitoring times, and in principle, the spot with the furthest distance is selected as the only origin spot.

Finally, we obtained the area burned and the spread vector of the forest fire, as well as had access to information on the area burned, the rate of spread in addition to the location, start time, and duration of the forest fires.

For instance, in 2018, the forest fire that occurred in Inner Mongolia and Heilongjiang Province (Figure 4) started at 14:00 on 1 June 2018, ended at 2:00 on 5 June 2018, and lasted for 4.5 days. It involved 188 fire spots with a spread rate of 6882.17 m/d and a burned area of 4741 ha.

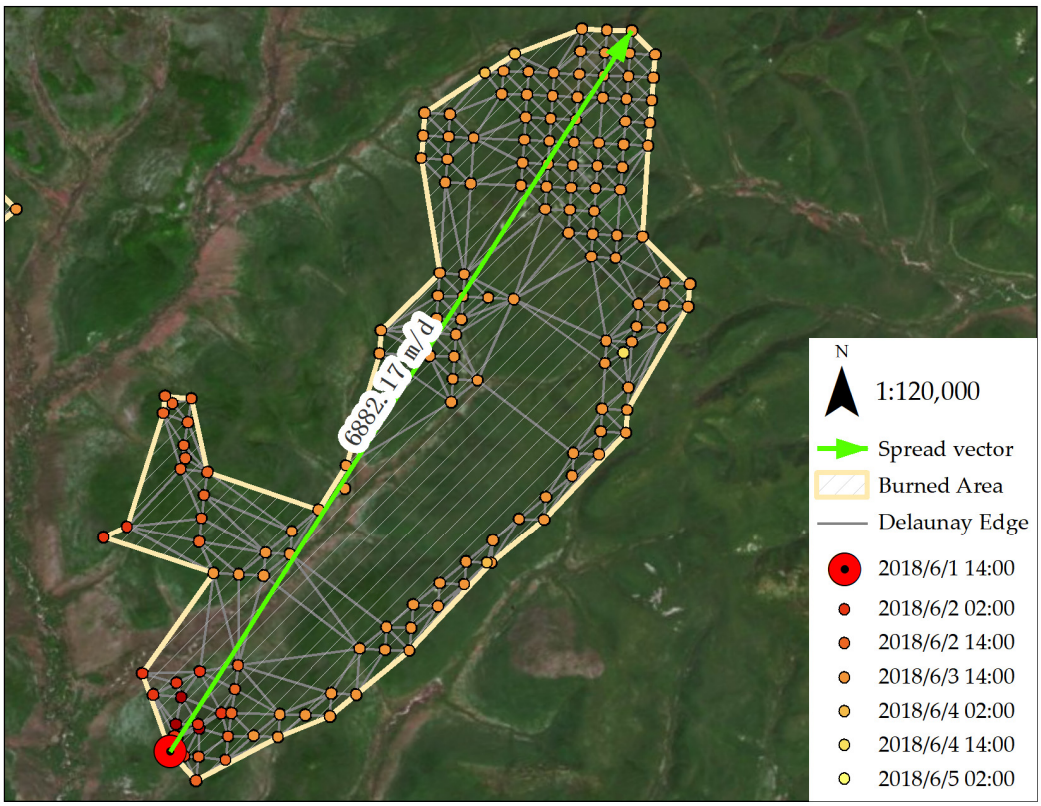

Figure 4. An example of results from spatiotemporal clustering and spread reconstruction: The forest fire in Inner Mongolia and Heilongjiang Province in 2018.

2.3.3. Method of Mathematical Statistics

After processing ten years of VIIRS active fire data in China (2012–2021), we were able to obtain forest fire spots, forest fire events, and large forest fire events. Through further calculations, we derived metrics such as the frequency of FFS, FFE, LFFE; duration; burned area; and spread rate. To measure the relationships among the primary information of these data (FFS, FFE, LFFE, and average area burned), we used a Pearson correlation coefficient (Pearson) analysis. A correlation coefficient closer to 1 or −1 indicates a stronger correlation, while a coefficient closer to 0 indicates a weaker correlation.

Forest fire metrics were compiled and organized into tables for each province and the five regions, creating a comprehensive database of information. First, we summarized the metrics FFS, FFE, LFFE, and area burned for each province and region. Then, statistical tables were created for the five regions, and maps were generated to analyze regional differences. We also calculated the annual and monthly FFS, FFE, LFFE, and burned area for the country and the five regions, and presented charts to show their temporal distribution. Finally, we analyzed the annual and monthly FFE of different durations and the monthly spread rates of LFFE, and presented appropriate charts to illustrate the findings.

3. Results and Discussion

3.1. Pearson Analysis

Based on the analysis of forest fire data in China, from 2012 to 2021, we finally obtained a total of 72.41×10^4 forest fire spots and detected a total of 7728 forest fire events, and of these, 1118 forest fire events were classified as large forest fire events. The total burned area of large forest fire events was 58.4×10^4 ha, with a minimum burned area of 6.9 ha, and an average burned area of 552 ha. Forest fire events filtered out 70.9% of forest fire spots. Large forest fire events filtered out 85.5% of forest fire events. These data demonstrate a large number of forest fire spots and the subsequent filtering process for notable events, allowing us to focus on the most important cases. Regarding the burned area, the scale and severity of large forest fire events are revealed. This provides valuable insights for research.

Forest fire metrics were summarized for each month of the 10-year period for five regions, and a total of 600 records were calculated. Using a Pearson analysis at a significance level of 0.01, we calculated the correlations among FFS, FFE, LFFE, and average burned area (Table 1) and found the following six main results:

1. The correlation coefficient between FFS and FFE is 0.957, indicating an extremely strong relationship between the two. This means that FFE can be accurately estimated from FFS, especially in situations in which obtaining direct measurements of FFE may be difficult. Overall, these findings highlight the importance of the relationship between FFS and FFE for effective forest fire management and prevention.
2. FFS and FFE have an extremely strong correlation. This indicates that, despite the condition filtering of 10 clustering spots during temporal and spatial clustering, the forest fire events obtained can still comprehensively reflect the occurrence of forest fires, not just in terms of space or time.
3. The correlation analysis shows that LFFE had strong correlations of 0.666 and 0.772 with FFS and FFE, respectively. These results suggest that by monitoring FFS and FFE, it may be possible to predict the likelihood of large forest fires occurring. This information could be very valuable in preventing and controlling large fires.
4. The correlation coefficients between the average burned area and FFS and FFE are 0.298 and 0.347, respectively, which are weak correlations. This suggests that burned areas may have different characteristics for forest fires compared to fire frequency, and therefore a comprehensive study of this metric is necessary. The burned area can provide more insights into the severity and intensity of forest fires.
5. The correlation coefficient between LFFE and the average burned area is 0.412, indicating a moderate positive relationship. This means that as LFFE increase, the average burned area also tends to increase, but the relationship is not very strong. It is crucial

to take into consideration other factors that could affect the area burned by a forest fire, such as topography, climate, vegetation type, and human activity.

6. Overall, the correlations among the different metrics highlight their validity and value in analyzing forest fires from various perspectives. By considering multiple indicators, we can gain comprehensive insights that help to improve our understanding of forest fire dynamics, enhance our ability to mitigate and prevent such events, and assist in the development of more effective strategies for their management.

Table 1. Results of Pearson analysis of the frequency of forest fires, and the average burned area for all years and months in the five regions.

Metrics	FFS	FFE	LFFE	Average Burned Area
FFS	1	0.957	0.666	0.298
FFE	0.957	1	0.772	0.347
LFFE	0.666	0.772	1	0.412
Average burned area	0.298	0.347	0.412	1

3.2. Spatial Characteristics

3.2.1. Five Regional Scales

We summarized four metrics (i.e., FFS, FFE, LFFE, and burned area) based on the five regions in Table 2 and conducted a comparative analysis of metrics data across regions to investigate regional differences in forest fires.

Table 2. Statistics on the frequency of forest fires and burned area for China and five regions.

Regions	Forest Area (10^6 ha)	Forest Cover (%)	FFS (10^4)	FFE	LFFE	Burned Area (10^4 ha)
Southern Region	81.19	49.10	35.5	3094	249	9.3
Southwest Region	43.00	45.30	18.6	2582	552	38.1
Northeast Region	33.47	42.40	10.9	1221	132	4.5
N-E-China	42.02	22.30	6.3	725	153	5.6
Northwest Region	41.75	9.70	1.2	106	32	0.81
China	220.45	22.96	72.41	7728	1118	58.4

In terms of the FFS and FFE metrics, the Southern Region had the highest values of 35.5×10^4 and 3094, accounting for 49.0% and 40.0% of the total, respectively. The Southwest Region ranked second with values of 18.6×10^4 and 2582, accounting for 25.6% and 33.4% of the total, respectively. The Northeast Region ranked third with values of 10.9×10^4 and 1221, followed by the N-E-China Region with values of 6.3×10^4 and 725, respectively. The Northwest Region had the lowest values of 1.2×10^4 and 106, respectively.

In terms of the LFFE and burned area metrics, the Southwest Region had the highest values of 552 and 38.1 × 104 ha, accounting for 49.3% and 65.3% of the total, respectively; the Southern Region ranked second with values of 249 and 9.3×10^4 ha, accounting for 22.4% and 16.0% of the total, respectively; the N-E-China Region ranked third with values of 153 and 5.6×10^4 ha, followed by the Northeast Region with values of 132 and 4.5×10^4 ha, respectively. The Northwest Region still had the lowest values of 32 and 0.81×10^4 ha, respectively.

There are obvious differences among the regional indicators in China, both in terms of frequency and scale. The sum of the four metrics (FFS, FFE, LFFE, burned area) in the Southern and Southwest Regions accounted for 74.6%, 73.4%, 71.7%, and 81.3%, respectively, indicating a distinct spatial aggregation of forest fires in China and exhibiting distribution patterns between more in the south and less in the north, and more in the east and less in the west. While forest fires are more frequent in the South Region, they tend to cause more extensive damage in the Southwest Region. These findings highlight significant regional variations in the characteristics and intensity of forest fire.

To further analyze the risk level of forest fires, we also calculated the proportion of large forest fires to forest fire events (defined as LFFE divided by FFE) as an expression of the probability of a forest fire developing into a large forest fire. The highest probability was in the Northwest Region at 30.2%, followed by 21.4% in the Southwest Region, 21.1% in the N-E-China Region, 10.8% in the Northeast Region, and surprisingly the lowest in the Southern Region at 8.0%. These findings suggest that forest fires in the Northwest Region are more prone to spreading and becoming large fires compared to other regions. In contrast, although the Southern Region has a high frequency of forest fires, most of them are small in size and have a lower chance of developing into large forest fires.

To better understand the relationship between forest fires and forest resources in China, Table 2 also includes information on forest area and forest cover. The South Region and Southwest Region have a combined forest area of 81.19×10^6 ha (with an average cover of 49.10%) and 43.00×10^6 ha (with an average cover of 45.30%), respectively, with a total proportion of 71.5%, and the percentage of the four metrics in the two regions is greater than 70%, which is consistent with the percentage of forest area. However, while the Southwest Region, N-E-China Region, and Northwest Region have similar forest areas of 43.00×10^6 ha, 42.02×10^6 ha, and 41.75×10^6 ha, respectively, the four forest fire metrics vary significantly, indicating a gradual decrease in forest cover. The Northeast Region has the smallest forest area of 33.47×10^6 ha, but its four forest fire metrics are relatively high, primarily due to its high forest cover. Therefore, the spatial distribution of forest fires in China is not only related to the area of forests in each region but also to their forest cover.

To analyze regional differences in forest fires from a more diverse perspective, we calculated forest fire frequency densities (defined as FFS, FFE, and LFFE divided by forest area) for each region. We found similar values of FFS in the Southern and Southwest Regions, and the highest values of FFE and LFFE in the Southwest Region. The FFE were comparable in the Southern and Northeast Regions, while the LFFE were higher in the Northeast and N-E-China Regions.

In conclusion, these data clearly demonstrate the spatial distribution differences of forest fires and the distinct characteristics they exhibit in terms of frequency and scale. For instance, the Southern Region shows a higher frequency of forest fires, but with smaller scales and a lower probability of developing into large forest fire events. Forest fire events in the Southwest Region are more likely to cause damage to forest resources. Although forest fire events in the Northwest Region occur less frequently, they have a higher potential to develop into large fires.

3.2.2. Provincial Scale

We counted and geographically visualized the four indicators (FFS, FFE, LFFE, and area burned) by provinces/municipalities, as shown in Figure 5. Comparisons among provinces for each indicator illustrate the distribution of forest fires at the provincial level. Within each province, comparisons among indicators reveal different perspectives of forest fires, such as frequency and size.

According to the FFS indicator map (Figure 5a), Yunnan Province, Guangxi Province, Heilongjiang Province, Guangdong Province, and Hunan Province were identified as the top provinces with values above 50,000, i.e., 14.4×10^4 (19.9%), 8.2×10^4, 6.7×10^4, 6.0×10^4, and 5.1×10^4, respectively. Similarly, based on the FFE indicator map (Figure 5b), Yunnan Province, Heilongjiang Province, Sichuan Province, and Guangdong Province emerged as the provinces with values above 500, i.e., 1994 (25.8%), 922, 584, and 562, respectively. Moreover, when examining the LFFE indicator map (Figure 5c) and the burned area indicator map (Figure 5d), Yunnan Province and Sichuan Province were found to have values above 100 and above 5×10^4 ha, i.e., 412 and 24×10^4 ha (36.9% and 41.8%) and 140 and 13.8×10^4 ha, respectively.

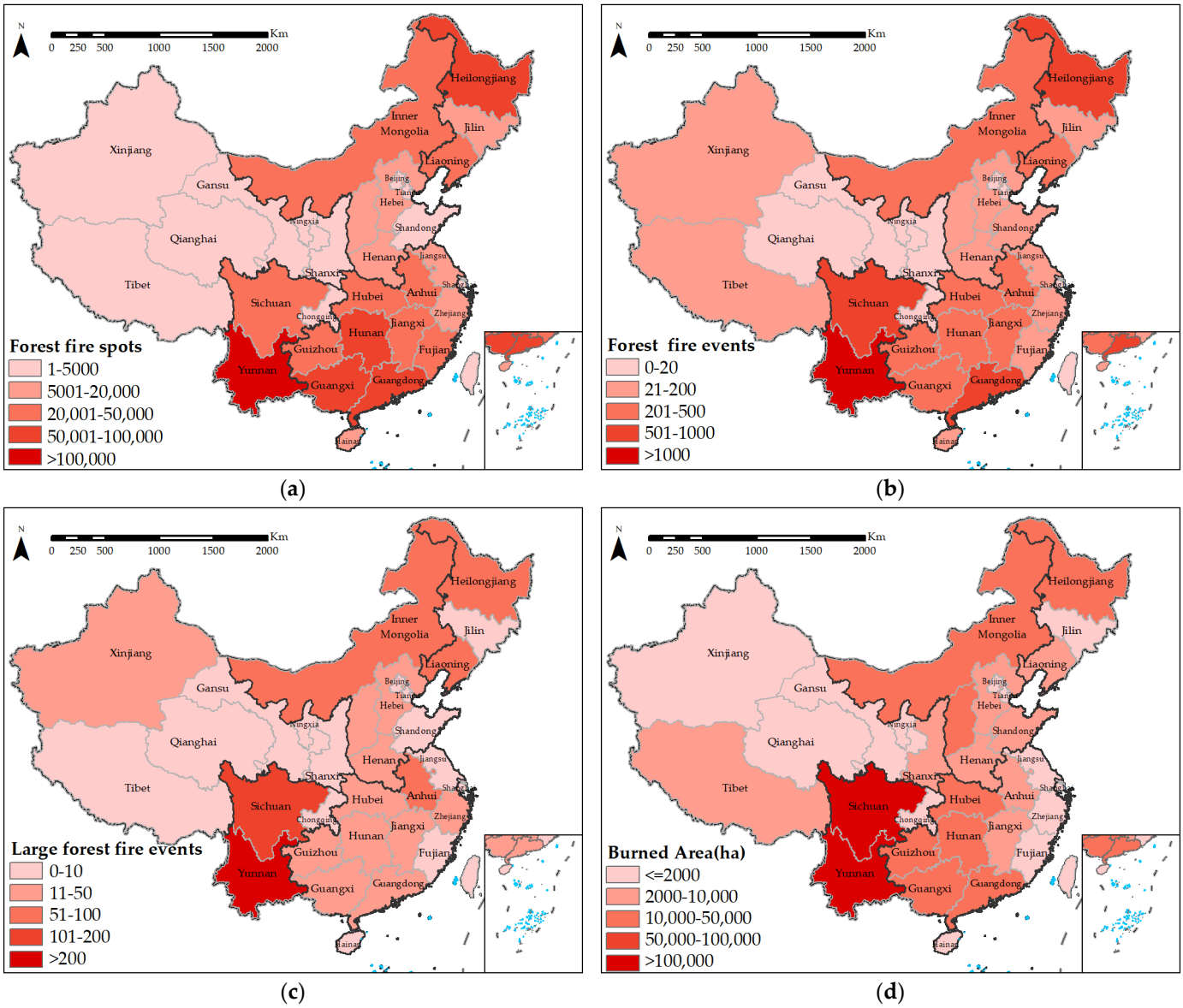

Figure 5. Map of Provincial distribution on: (**a**) Frequency of forest fire spot, (**b**) frequency of forest fire events, (**c**) frequency of large forest fire events, (**d**) burned area.

The FFS indicator map (Figure 5a) shows that the provinces with a high frequency of forest fire spots are concentrated in the northeast and south of China, while the provinces in the northwest have a very low frequency of forest fire spots. A similar pattern applies to the other indicator maps (Figure 5b–d). However, there are also intensity differences between these indicators. When comparing the indicators for each province, Yunnan Province stands out as the most prominent province, exhibiting the highest values across all four indicators and exerting a substantial influence on the overall characteristics of forest fires. There are also differences in the intensities of the four indicators in the same province. For instance, in Sichuan Province, there is a progressive increase in intensity from FFS (Figure 5a) to burned area (Figure 5d), as indicated by the color shades. Additionally, provinces in the Southern Region generally display higher intensities in terms of FFS and FFE (Figure 5a,b), while exhibiting a distinctly lower intensity in terms of LFFE (Figure 5c).

In the Southern Region, Guangxi Province has the highest FFS, with 8.2×10^4, accounting for 23% of the region; Guangdong Province has the highest FFE with 562, accounting for 18.2% of the region; Anhui Province has the highest LFFE with 62, accounting for 24.8% of the region; Hubei Province has the largest burned area with 2.2×10^4 ha, accounting

for 23.9% of the region. In contrast, the lowest FFS, FFE, LFFE, and burned area are from Jiangsu Province with 0.6×10^4, 31, 1, and 19 ha, respectively. As a result, the intensity of the indicators is not consistent across the provinces in the region's performance.

In the Southwest Region, Yunnan Province has the highest values of the four metrics, accounting for 77.6%, 77.2%, 74.6%, and 64.0% of the region, respectively. The average burned area in Yunnan is 592 ha. The metrics in Sichuan Province are smaller than in Yunnan Province, but the average burned area is 979 ha, indicating that the average size of forest fires in Sichuan is larger than in Yunnan.

In the Northeast Region, forest fires are primarily concentrated in Heilongjiang, where the four metrics of 6.7×10^4, 922, 75 and 4.0×10^4 ha, respectively, accounting for 61.4%, 75.5%, 56.8%, and 88.8% of the region, with an average burned area of 537 ha. In the N-E-China Region, Inner Mongolia has the highest values of the four metrics, with 3.0×10^4, 382, 75, and 3.3×10^4 ha, respectively, accounting for 47.6%, 52.7%, 49.0%, and 59.3% of the region, with an average burned area of 444 ha. In the Northwest Region, Shaanxi has the highest FFS, with 4000, accounting for 32.6% of the region; Xinjiang has the highest FFE and LFFE at 50 and 21, respectively, accounting for 47.2% and 65.5% of the region; and Tibet has the largest burned area with 3292 ha.

As a result, forest fires exhibit a high degree of inter-provincial aggregation and inconsistent intensity among the indicators within provinces. In addition, there are provinces in each region where the frequency of forest fires and the area burned are prominent.

3.3. Spatiotemporal Characteristics

3.3.1. Annual Analyses

The FFS, FFE, LFFE, and burned area metrics of China and the five regions were counted over the years to analyze the trend and characteristics of inter-annual forest fires (Figure 6).

In China (all the red bar charts in Figure 6 correspond to the right axis), the peak year for all four metrics (i.e., FFS, FFE, LFFE, burned area) was 2014, with values of 11.5×10^4, 1344, 202, and 11.0×10^4 ha that accounted for 15.9%, 15.4%, 18.1%, and 18.9% of the total, respectively. The lowest year for all four metrics was 2018, with values of 5.2×10^4, 480, 67, and 2.0×10^4 ha that accounted for 7.1%, 6.2%, 6.0%, and 3.5% of the total, respectively. Although the FFS, FFE, LFFE metrics had subpeaks in 2013, with values of 10.5×10^4, 1158, and 185 that accounted for 14.5%, 15.0%, and 16.5% of the total, respectively, the subpeak year for burned area was in 2020, with a value of 10.8×10^4 ha that accounted for 18.4% of the total.

The average annual values of FFS, FFE, and LFFE for China were calculated, and the average FFS was 7.2×10^4. The years 2012–2015 represented a concentrated period of high forest fires in China, with a cumulative FFS of 37.4×10^4, accounting for 51.6% of the total. The annual average during that period was 9.3×10^4. From 2016 to 2021, the cumulative FFS was 35.0×10^4, with an annual average of 5.8×10^4, representing a decrease of 37.5% compared to the annual average for 2012–2015. Similar trends were observed for FFE and LFFE, i.e., the metrics from 2012 to 2015 were higher (4286 and 604, respectively) compared to the metrics from 2016 to 2021 (i.e., 1071 vs. 151, respectively). This indicates a significant decline in both forest fire events and large forest fire events in China since 2015.Therefore, at a national scale, the overall trends for FFS, FFE, and LFFE were similar from 2012 to 2021, with an initial increase followed by a decrease, reaching a peak in 2014, and exhibiting slight fluctuations in 2017 and 2019, but showing an overall decreasing trend. The overall inter-annual trend in burned area substantially differs from the three metrics mentioned above. In 2020, the burned area exhibited notably higher values and displayed sharp differences from nearby years, suggesting the occurrence of larger fires and indicating that burned area is episodic.

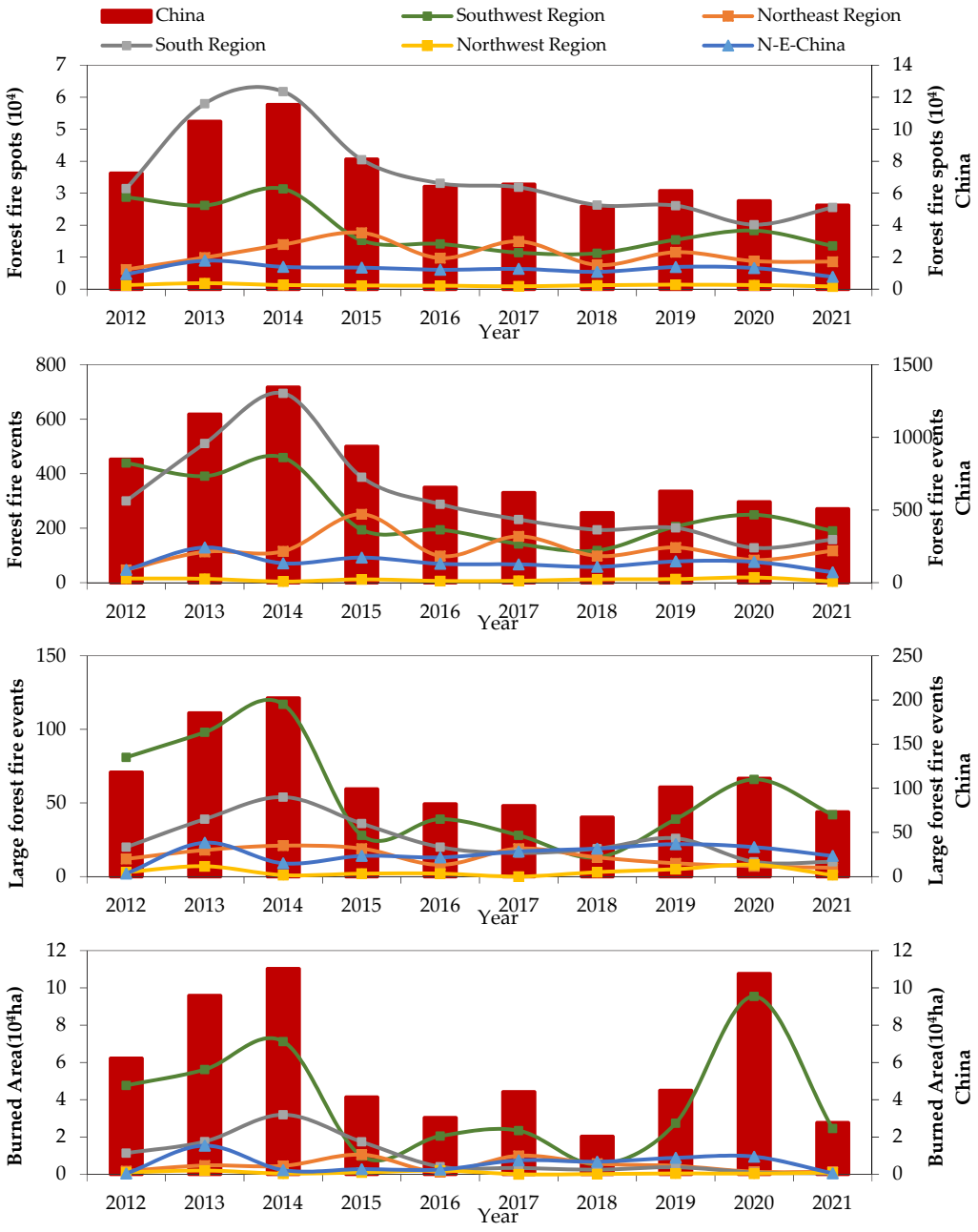

Figure 6. Annual frequencies of forest fire spots (FFS), forest fire events (FFE), and large forest fire events (LFFE), and burned area values of China and the five regions.

In five regions (all the line charts in Figure 6 correspond to the left axis), we obtained three main pieces of information. Firstly, excluding 2012 and 2020, the Southern Region had the highest FFS and FFE in other years, accounting for 42.5–55.3% of FFS and 31.2%–51.7% of FFE. Additionally, the Southwest Region had the highest LFFE, burned area (except for 2015 and 2018) in other years, accounting for 35–68.6% of the LFFE in calendar years and 52.9–88.7% of the burned area in calendar years. It is evident that forest fires in the Southern and Southwestern Regions were extremely conspicuous in all years and had a decisive influence on the national inter-annual trends. Secondly, the Northeast Region shows fluctuating inter-annual variations in each metric. The FFS and FFE both show peaks in 2015, 2017, and 2019 and troughs in 2016, 2018, and 2020, and the overall 10-year variation is small, with the FFS from 5.8% to 16.2%, showing only a difference between the maximum and minimum values of 10.4%. Thirdly, there are differences in the years of high forest fires among the five regions. The peak year for FFS, FFE, and LFFE in the Southern

and Southwest Regions was 2014, the peak year for the metrics in the Northeast Region was 2015, and the peak year for the metrics in the N-E-China Region and the Northwest Region was 2013.

Furthermore, it is worth noting that the Northwest and Northeast Regions consistently had lower FFS and FFE values with relatively minor fluctuations over the decade. In contrast, the Southwest Region experienced a significantly higher burned area in 2020, reaching 9.5 $\times$ 10^4 ha, which accounted for 88.7% of the total burned area for that year. This indicates a severe outbreak of forest fires in the Southwest Region in 2020. Notably, 2020 also marked the peak year for burned area in the Southwest Region, comprising 25.0% of the total burned area for that region.

3.3.2. Monthly Analyses

We summarized the monthly metrics (FFS, FFE, LFFE, and burned area) for China and five regions (Figure 7) to analyze and discuss the monthly distribution characteristics of forest fires.

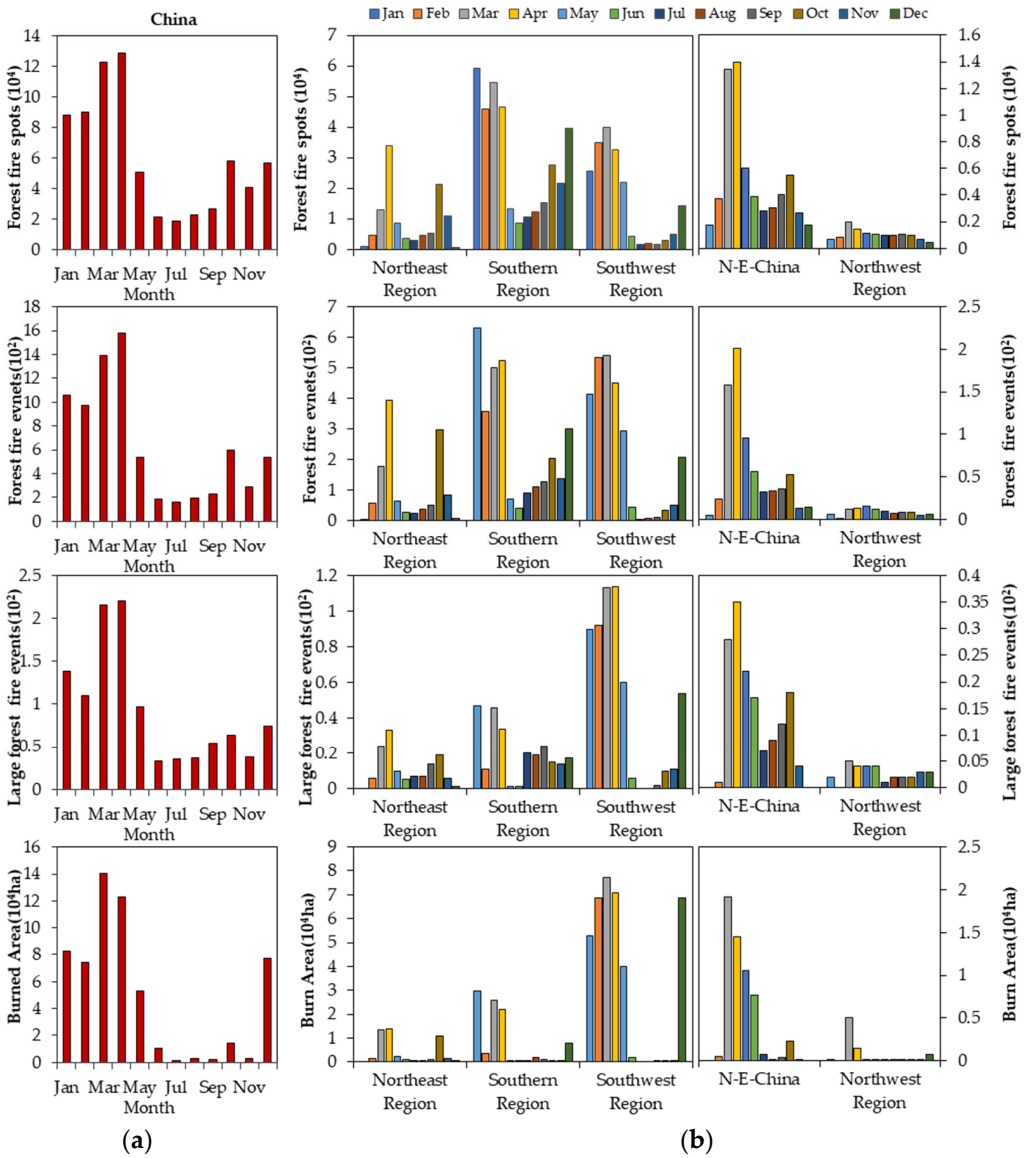

Figure 7. Monthly frequency of forest fire spots (FFS), frequency of forest fire events (FFE), frequency of large forest fire events (LFFE), and burned area: (**a**) In China; (**b**) in the five regions.

In China (left chart in Figure 7), the months of March and April exhibit high concentrations of forest fires. The metrics for these months include FFS (12.2 × 104 (16.9%)), FFE (1389 (18.0%)), LFFE (216 (19.7%)), and burned area (14.1 × 104 ha (24.5%)) in March and FFS (12.8 × 104 (17.7%)), FFE (1579 (20.4%)), LFFE (220 (19.7%)), and burned area (12.3 × 104 ha (24.1%)) in April. Together, March and April account for a significant percentage of forest fires throughout the year, with a total of 34.6%, 38.4%, 39.4%, and 48.6% for the respective metrics. This indicates a higher concentration of forest fire events and large forest fires during these two months, with nearly half of the total burned area occurring in March and April. Additionally, January, February, May, October, and December also exhibit higher metrics for forest fires in China. The values for FFS for these months were 8.8×10^4, 9.0×10^4, 5.1×10^4, 5.8×10^4, and 5.6×10^4 respectively. Conversely, the period from June to September shows lower forest fire metrics, with the highest value of FFS being 2.7×10^4, the highest value of FFE being 230, the highest value of LFFE being 54, and the highest value of burned area being 1.0×10^4 ha.

We analyzed the indicators by season in China and observed significant seasonal differences in forest fires as follows: Spring (March, April, and May) has the highest values of the metrics, followed by winter (December, January, and February), autumn (September, October, and November), and summer (June, July, and August). As an illustration, the value of FFS reaches 30.2×10^4 (41.6%) in spring, followed by 23.4×10^4 (32.3%) in winter, 12.6×10^4 (17.4%) in autumn, and 6.7×10^4 (8.7%) in summer. Therefore, most forest fires in China occur in spring and winter. The higher incidence in these seasons can be attributed to the dry and cold climate, low rainfall, and the presence of dead branches on forested land.

In five regions (middle and right chart in Figure 7), variations in the peak month and duration of concentrated high occurrence months are observed. Taking FFS as an example, in the Southern Region, the peak month was January with 5.9×10^4 (16.7% of the total), followed by March, April, February, and December. The concentrated high occurrence months span from December to April, accounting for 69.2% of the total. In the Southwest Region, the peak month was March with 4×10^4 (21.5% of the total), followed by February, April, January, and May. The concentrated high occurrence months were five months in total (January to May), accounting for a combined total of 83.2%. In the Northeast Region, the peak month was April with 3.4×10^4 (31.0% of the total), followed by October. The concentrated high occurrence months span from April to October, accounting for 50.1% of the total. In the N-E-China Region, the highest occurrence months were March and April, with metrics of 1.3×10^4 and 1.4×10^4, respectively, which accounted for a combined total of 43.9%. In the Northwest Region, the highest occurrence month was March, with 0.2×10^4 (16.3% of the total).

Overall, the peak months and concentrated high occurrence months for the remaining metrics were generally consistent with those of FFS, with some minor differences, such as that the LFFE and burned area in the Southern Region did not show a high occurrence in February. Additionally, the Northeast Region had a larger burned area in March, and the peak month of burned area in the N-E-China Region was also in March.

In December, the metrics for FFS, FFE, and LFFE were not significant, but the burned area was relatively high. The FFS only accounted for 7.8% of the total, with a value of 5.6×10^4, while the burned area accounted for 13.2% of the total, with a value of 7.7×10^4 ha. However, in the Southwest Region, the burned area in December was 6.8×10^4 ha, accounting for 88.7% in that month. The average burned area in December for the region was 1267 ha, which was 1.8 times higher than the average burned area (691 ha) for the entire region. Moreover, this was also the highest monthly average burned area among all regions. Through comprehensive annual and monthly analysis, it can be concluded that a large forest fire occurred in the Southwest Region in December 2020.

3.3.3. Duration Analyses

The total frequency of forest fire events was 7728, of which 10.9% lasted less than 12 h, 29.4% lasted between 12 h and 2 d, 34.3% lasted between 2 d and 5 d, and 25.3% lasted longer than 5 d, with 851, 2270, 2653, and 1954 forest fire events, respectively (Figure 8).

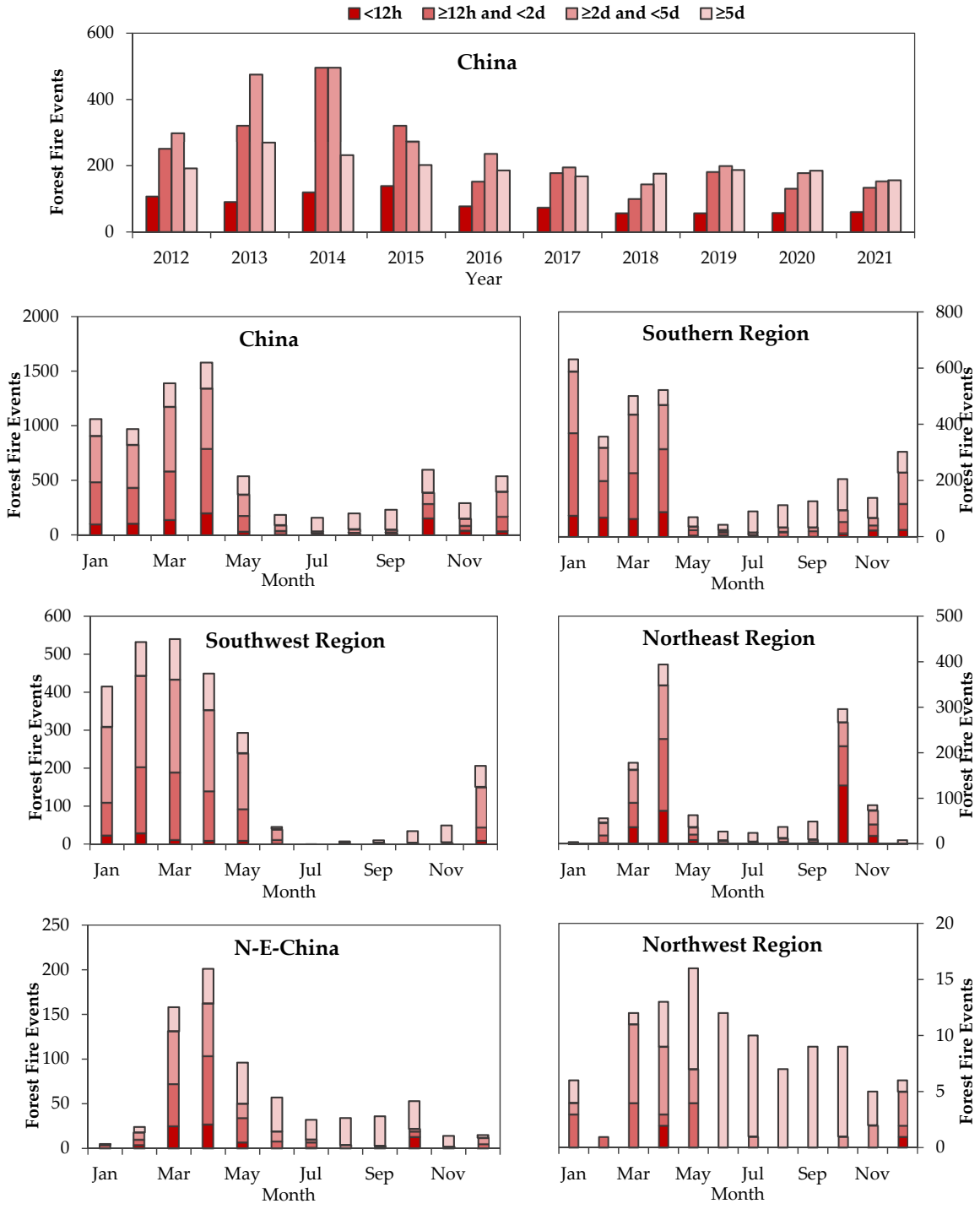

Figure 8. Inter-annual distribution of FFE in China for different durations; inter-monthly distribution of FFE in five regions for different durations.

On the one hand, the majority of FFE in all years had a duration ranging from 12 h to 5 days, with proportions ranging from 51.2% to 73.7%. These fires impacted the overall trends of forest fires in China and exhibited consistent annual and monthly distributions.

On the other hand, forest fires with a duration of less than 12 h in all year were the least, ranging from 7.9% to 15.0%. This can be attributed to the filtering process that removes short duration burning fires with fewer than 10 spots during spatiotemporal clustering.

The annual variation in FFE for durations greater than 5 d was relatively stable, i.e., from 8.0% to 13.8%, with a variation of only 5.8%. The monthly variation in these forest fires was also relatively stable, increasing from 4.7% to 12.2%, with a variation of only 7.5%. As a result, there is an episodic characteristic to the long-burning forest fires, with no obvious annual or monthly concentration.

When analyzing the duration of forest fires lasting between 12 h and 5 days in different regions, the Southern, Southwest, and Northeast Regions have a higher proportion of forest fires within this duration, with 63.2%, 72.8%, and 56.8% of forest fires in this duration, respectively, and their monthly distribution is consistent with the monthly distribution of overall FFE in each region, with the proportion of forest fires exceeding 50%. The proportions of forest fires within this duration were relatively smaller in the N-E-China Region and Northwest Region, at 49.4% and 35.8%, respectively. Those in the N-E-China Region were concentrated in March and April, with a total of 67.3%. Those in the Northwest Region were concentrated in March, April, and May, with a total of 65.8%.

Regarding forest fires lasting more than 5 days, the Southern, Southwest, Northeast, N-E-China, and Northwest Regions experienced 759, 595, 248, 287, and 65 such forest fire events, accounting for 24.5%, 23%, 20.3%, 39.6%, and 61.3%, respectively. In the Southern Region, the monthly average is 63 forest fire events, with the percentage of calendar months varying from 2.4% to 14.6%, with a variation of only 12.2%, and the fewest forest fire events occurred in June, with 18 FFE. In the Southwest Region, the monthly average was 49 FFE, with the majority occurring between October and May. There were over 30 forest fire events in all months during this period, but less than 10 FFE in all other months, with considerably variation. In the Northeast Region, the monthly average was 20 FFE, with most fires occurring between April and October. In the N-E-China Region, the monthly average was 23 FFE, with the majority of fires occurring between March and October. The Northwest Region had 61.3% of such forest fires, indicating that they were more likely to spread and to burn continuously here; the monthly average was 5 FFE, concentrated mainly between May and October. In summary, the concentration of forest fire events in this category spans a wide range of months, with little monthly concentration and relatively minor differences between months.

3.3.4. Spread Rate Analyses

The average spread rate of large forest fire events in China shows considerable variation from month to month (Figure 9), with the overall peak spread rate in March at 1808 m/d, followed by higher spread rates in January (1622 m/d), February (1567 m/d), April (1249 m/d), and December (1393 m/d), with an average spread rate of 1523 m/d for these seven months and 310 m/d for the remaining five lower months, which is only 20% of the former. The monthly distribution of higher rates is broadly consistent with the monthly distribution of FFS, FFE, and LFFE in China (Figure 6), where forest fires also have high rates of spread during periods of high forest fire concentration.

This study examined the average rates of forest fire spread in five regions. In the Southwest Region, the average spread rate was 1315 m/d, and the peak spread rate was in February at 1663 m/d, followed by December (1650 m/d), January (1597 m/d), June (1545 m/d), May (1466 m/d), March (1304 m/d), and April (1211 m/d). In the Southern Region, the average spread rate was 697 m/d, and the peak spread rate was in May at 2684 m/d, followed by March (1965 m/d), January (1859 m/d), April (1821 m/d), February (1374 m/d), and December (1013 m/d), In the Northeast Region, spread rates exceeding 1000 m/d were concentrated in March (4341 m/d), April (1498 m/d), and October (1206 m/d), with an average spread rate of 856 m/d. In the N-E-China Region, with an average spread rate of 539 m/d, only March (2382 m/d) and February (1626 m/d) exceeded 1000 m/d. The Northwest Region had the lowest average spread rate of 368 m/d,

but with a peak spread rate of 2431 m/d in March. March had the fastest spread rate in the Northeast Region, and seven months in the Southwest Region had high values for spread rates exceeding 1000 m/d.

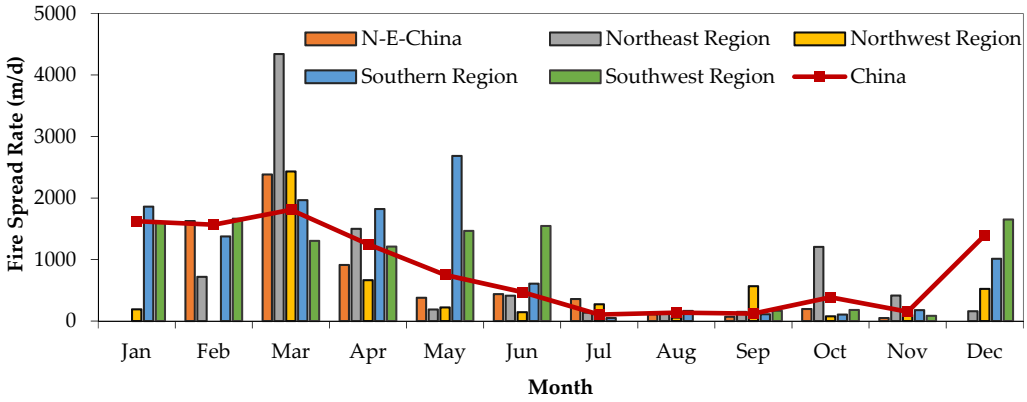

Figure 9. Monthly averages of forest fire spread rate for counter performances in China and in five regions.

In summary, the Southwest Region had the longest period of high fire spread rate, lasting 7 months, followed by the Southern Region, which lasted for 6 months. These regions are both located in the southern part of China and have similar characteristics, with stronger fire spread in spring and winter. The fastest fire spread rate in the Northeast Region occurred in March, followed by October. Similar to this region, the N-E-China Region and Northwest Region also experienced stronger forest fire spread in spring and autumn. The spread of a forest fire can also represent the danger of a forest fire, and the characteristics of the rate of spread can help to develop different levels of fire policy for different months.

4. Conclusions

In this study, we utilize VIIRS active fire data in China from 2012 to 2021 to identify forest fire spots, forest fire events, and large-scale forest fire events through spatial extraction, spatial and temporal clustering, and spread reconstruction. To filter out sporadic, smaller, and incomplete fires, forest fire events were selected based on spots greater than 10, and reconstructed forest fire events were selected based on spots greater than 20 and a duration of more than 2 days, representing larger forest fires. In practice, a reconstructed forest fire event has a minimum burned area of 6.9 ha, which is classified as a larger forest fire according to China's forest fire classification.

This study represents a novel attempt aimed at extracting more fire information from VIIRS active fire data to describe fire characteristics. However, there are several limitations that need to be acknowledged.

Firstly, there is uncertainty associated with the VIIRS active fire data used in this study [20,44], which is due to a traditional challenge with optical remote sensing products, namely the difficulty in effectively observing in rainy, cloudy, and heavily hazy weather conditions. In addition, due to the coarse temporal resolution of VIIRS data, some fast-burning forest fires with durations less than 12 h may have been missed. There is also the potential for misclassification due to problems with the fire detection algorithm. However, these errors are unlikely to introduce significant bias into remote sensing monitoring data [44], as shown in other studies [42,45]. Secondly, the data processing methods in this study have certain uncertainties. For instance, the clustering of active fires to form forest fire events and the reconstruction of spread have undifferentiated spatial and temporal thresholds. These thresholds are empirical values that require further refinement and optimization, taking into consideration the seasonal, regional, and size variations of forest fires. The estimation of the duration of forest fire events may be biased due to the temporal

resolution of the VIIRS data. The Delaunay triangle method used for reconstructing the extent burned area may overestimate by including unburned patches, despite using island thresholds. The average rate of spread may be underestimated, and estimating the origin spot of a fire can be challenging. Despite these limitations, the estimates of various statistical quantities provide objective and consistent insights into forest fire characteristics. Therefore, future studies should consider these limitations and work towards refining and optimizing the methods for processing forest fire data.

Furthermore, this study lacks additional historical information for validation and assessment. The current records of ground-based observations of forest fires are incomplete and inconsistent, making it challenging to accurately evaluate and calibrate the results of forest fire statistics. Therefore, it is suggested that, in the future, a forest fire information database should be established as a uniform standard of detailed observation records for forest fires, which should be implemented nationwide to better support forest fire research in China.

In summary, this study focuses on the spread rate and area of forest fires, but overlooks other important characteristics such as spread direction and distance. Further research is necessary to explore how these additional spread characteristics can enhance the characterization of forest fires in China. Future studies can delve into analyzing the drivers of forest fires and predicting their development using the data obtained. Overall, this study provides valuable research ideas and serves as a foundational dataset for investigating fire behavior and predicting forest fires. The methods used can also serve as a reference for future forest fire research utilizing remote sensing data.

Author Contributions: Conceptualization, methodology, B.D.; validation, J.X.; formal analysis, investigation, B.D.; resources, C.H.; data curation, C.H.; writing—original draft preparation, B.D.; writing—review and editing, B.D. and S.Z.; visualization, B.D.; supervision, J.X.; project administration, S.Z.; funding acquisition, H.L. All authors have read and agreed to the published version of the manuscript.

Funding: This research is supported by a key project of the National Natural Science Foundation of China, "Research on the Concept Shift of Spatial data flow", with the support number 41571394.

Institutional Review Board Statement: Not applicable.

Informed Consent Statement: Not applicable.

Data Availability Statement: The data used in the study are available from the authors and can be shared upon reasonable requests.

Acknowledgments: All authors are grateful to anonymous reviewers and editors for their constructive comments on earlier versions of the manuscript.

Conflicts of Interest: The authors declare no conflict of interest.

References

1. Giglio, L.; Randerson, J.T.; van der Werf, G.R. Analysis of daily, monthly, and annual burned area using the fourth-generation global fire emissions database (GFED4). *J. Geophys. Res. Biogeosci.* **2013**, *118*, 317–328. [CrossRef]
2. Alkhatib, A.A. A review on forest fire detection techniques. *Int. J. Distrib. Sens. Netw* **2014**, *10*, 597368. [CrossRef]
3. Van Der Werf, G.R.; Randerson, J.T.; Giglio, L.; Collatz, G.J.; Mu, M.; Kasibhatla, P.S.; Morton, D.C.; Defries, R.S.; Jin, Y.; Van Leeuwen, T.T. Global fire emissions and the contribution of deforestation, savanna, forest, agricultural, and peat fires (1997–2009). *Atmos. Chem. Phys.* **2010**, *10*, 11707–11735. [CrossRef]
4. Cardil, A.; Molina-Terren, D. Factors Causing Victims of Wildland Fires in Spain (1980–2010). *Hum. Ecol. Risk Assess. Int. J.* **2015**, *21*, 67–80. [CrossRef]
5. Diakakis, M.; Xanthopoulos, G.; Gregos, L. Analysis of forest fire fatalities in Greece: 1977–2013. *Int. J. Wildland Fire* **2016**, *25*, 797–809. [CrossRef]
6. Balch, J.K.; Bradley, B.A.; Abatzoglou, J.T.; Nagy, R.C.; Fusco, E.J.; Mahood, A.L. Mahood Adam L. Human-started wildfires expand the fire niche across the United States. *Proc. Natl. Acad. Sci. USA* **2017**, *114*, 2946–2951. [CrossRef] [PubMed]
7. Pechony, O.; Shindell, D.T. Driving forces of global wildfires over the past millennium and the forthcoming century. *Proc. Natl. Acad. Sci. USA* **2010**, *107*, 19167–19170. [CrossRef]

8. Cardil, A.; Eastaugh, C.S.; Molina-Terren, D. Extreme temperature conditions and wildland fires in Spain. *Theor. Appl. Climatol.* **2015**, *122*, 219–228. [CrossRef]
9. Taylor, A.H.; Trouet, V.; Skinner, C.N.; Stephens, S. Socioecological transitions trigger fire regime shifts and modulate fire-climate interactions in the Sierra Nevada, USA, 1600–2015 CE. *Proc. Natl. Acad. Sci. USA* **2016**, *113*, 13684–13689. [CrossRef] [PubMed]
10. Westerling, A.L.; Hidalgo, H.G.; Cayan, D.R.; Swetnam, T.W. Warming and Earlier Spring Increase Western U.S. Forest Wildfire Activity. *Science* **2006**, *313*, 940–943. [CrossRef] [PubMed]
11. Jolly, W.M.; Cochrane, M.A.; Freeborn, P.H.; Holden, Z.A.; Brown, T.J.; Williamson, G.J.; Bowman, D.M.J.S. Climate-induced variations in global wildfire danger from 1979 to 2013. *Nat. Commun.* **2015**, *6*, 7537. [CrossRef]
12. Bowman, D.M.J.S.; Balch, J.K.; Artaxo, P.; Bond, W.J.; Carlson, J.M.; Cochrane, M.A.; D'Antonio, C.M.; DeFries, R.S.; Doyle, J.C.; Harrison, S.P.; et al. Fire in the Earth System. *Science* **2009**, *324*, 481–484. [CrossRef] [PubMed]
13. Archibald, S.; Staver, A.C.; Levin, S.A. Evolution of human-driven fire regimes in Africa. *Proc. Natl. Acad. Sci. USA* **2012**, *109*, 847–852. [CrossRef] [PubMed]
14. Keeley, J.E.; Syphard, A.D. Climate Change and Future Fire Regimes: Examples from California. *Geosciences* **2016**, *6*, 37. [CrossRef]
15. Wei, X.; Wang, G.; Chen, T.; Hagan, D.F.T.; Ullah, W. A Spatio-Temporal Analysis of Active Fires over China during 2003–2016. *Remote Sens.* **2020**, *12*, 1787. [CrossRef]
16. Andela, N.; Morton, D.C.; Giglio, L.; Paugam, R.; Chen, Y.; Hantson, S.; van der Werf, G.R.; Randerson, J.T. The Global Fire Atlas of individual fire size, duration, speed and direction. *Earth Syst. Sci. Data* **2019**, *11*, 529–552. [CrossRef]
17. Schroeder, W.; Oliva, P.; Giglio, L.; Quayle, B.; Lorenz, E.; Morelli, F. Active fire detection using Landsat–8/OLI data. *Remote Sens. Environ* **2016**, *185*, 210–220. [CrossRef]
18. Li, P.; Xiao, C.; Feng, Z.; Li, W.; Zhang, X. Occurrence frequencies and regional variations in Visible Infrared Imaging Radiometer Suite (VIIRS) global active fires. *Glob. Chang. Biol.* **2020**, *26*, 2970–2987. [CrossRef]
19. Giglio, L.; Csiszar, I.; Justice, C.O. Global distribution and seasonality of active fires as observed with the Terra and Aqua Moderate Resolution Imaging Spectroradiometer (MODIS) sensors. *J. Geophys. Res. Biogeosci.* **2006**, *111*, G02016. [CrossRef]
20. Hantson, S.; Padilla, M.; Corti, D.; Chuvieco, E. Strengths and weaknesses of MODIS hotspots to characterize global fire occurrence. *Remote Sens. Environ.* **2013**, *131*, 152–159. [CrossRef]
21. van der Werf, G.R.; Randerson, J.T.; Giglio, L.; van Leeuwen, T.T.; Chen, Y.; Rogers, B.M.; Mu, M.; van Marle, M.J.E.; Morton, D.C.; Collatz, G.J.; et al. Global fire emissions estimates during 1997–2016. *Earth Syst. Sci. Data* **2017**, *9*, 697–720. [CrossRef]
22. Thorsteinsson, T.; Magnusson, B.; Gudjonsson, G. Large wildfire in Iceland in 2006: Size and intensity estimates from satellite data. *Int. J. Remote Sens.* **2011**, *32*, 17–29. [CrossRef]
23. Yaduvanshi, A.; Srivastava, P.K.; Pandey, A. Integrating TRMM and MODIS satellite with socio-economic vulnerability for monitoring drought risk over a tropical region of India. *Phys. Chem. Earth* **2015**, *83–84*, 14–27. [CrossRef]
24. Giglio, L.; Descloitres, J.; Justice, C.O.; Kaufman, Y.J. An Enhanced Contextual Fire Detection Algorithm for MODIS. *Remote Sens. Environ.* **2003**, *87*, 273–282. [CrossRef]
25. Schroeder, W.; Oliva, P.; Giglio, L.; Csiszar, I.A. The New VIIRS 375m active fire detection data product: Algorithm description and initial assessment. *Remote Sens. Environ.* **2014**, *143*, 85–96. [CrossRef]
26. Aragão, L.E.O.C.; Anderson, L.O.; Fonseca, M.G.; Rosan, T.M.; Vedovato, L.B.; Wagner, F.H.; Silva, C.V.J.; Silva Junior, C.H.L.; Arai, E.; Aguiar, A.P.; et al. 21st Century drought-related fires counteract the decline of Amazon deforestation carbon emissions. *Nat. Commun.* **2018**, *9*, 536. [CrossRef]
27. Van Leeuwen, T.T.; van der Werf, G.R.; Hoffmann, A.A.; Detmers, R.G.; Rücker, G.; French, N.H.F.; Archibald, S.; Carvalho, J.A., Jr.; Cook, G.D.; de Groot, W.J.; et al. Biomass burning fuel consumption rates: A field measurement database. *Biogeosciences* **2014**, *11*, 7305–7329. [CrossRef]
28. Lian, C.; Xiao, C.; Feng, Z. Spatiotemporal Characteristics and Regional Variations of Active Fires in China since 2001. *Remote Sens.* **2022**, *15*, 54. [CrossRef]
29. Zhuang, Y.; Li, R.; Yang, H.; Chen, D.; Chen, Z.; Gao, B.; He, B. Understanding Temporal and Spatial Distribution of Crop Residue Burning in China from 2003 to 2017 Using MODIS Data. *Remote Sens.* **2018**, *10*, 390. [CrossRef]
30. Ke, H.; Gong, S.; He, J.; Zhou, C.; Zhang, L.; Zhou, Y. Spatial and temporal distribution of open bio-mass burning in China from 2013 to 2017. *Atmos. Environ.* **2019**, *210*, 156–165. [CrossRef]
31. Müller, D.; Suess, S.; Hoffmann, A.A.; Buchholz, G. The value of satellite–based active fire data for monitoring, reporting and verification of REDD+ in the Lao PDR. *Hum. Ecol.* **2013**, *41*, 7–20. [CrossRef]
32. Xie, H.; Du, L.; Liu, S.; Chen, L.; Gao, S.; Liu, S.; Pan, H.; Tong, X. Dynamic Monitoring of Agricultural Fires in China from 2010 to 2014 Using MODIS and GlobeLand30 Data. *ISPRS Int. J. Geo-Inf.* **2016**, *5*, 172. [CrossRef]
33. Tian, X.; Zhao, F.; Shu, L.; Wang, M. Distribution characteristics and the influence factors of forest fires in China. *For. Ecol. Manag.* **2013**, *310*, 460–467. [CrossRef]
34. Tian, Y.; Wu, Z.; Bian, S.; Zhang, X.; Wang, B.; Li, M. Study on Spatial-Distribution Characteristics Based on Fire-Spot Data in Northern China. *Sustainability* **2022**, *14*, 6872. [CrossRef]
35. Li, W.; Li, P.; Feng, Z. Delineating Fire-Hazardous Areas and Fire-Induced Patterns Based on Visible Infrared Imaging Radiometer Suite (VIIRS) Active Fires in Northeast China. *Remote Sens.* **2022**, *14*, 5115. [CrossRef]
36. Veraverbeke, S.; Sedano, F.; Hook, S.J.; Randerson, J.T.; Jin, Y.; Rogers, B.M. Mapping the daily progression of large wildland fires using MODIS active fire data. *Int. J. Wildland Fire* **2014**, *23*, 655–667. [CrossRef]

37. Loboda, T.; Csiszar, I. Reconstruction of fire spread within wildland fire events in Northern Eurasia from the MODIS active fire product. *Glob. Planet. Chang.* **2006**, *56*, 258–273. [CrossRef]
38. Cardíl, A.; Tapia, V.M.; Monedero, S.; Quiñones, T.; Little, K.; Stoof, C.R.; Ramirez, J.; De-Miguel, S. Characterizing the rate of spread of large wildfires in emerging fire environments of northwestern Europe using Visible Infrared Imaging Radiometer Suite active fire data. *Nat. Hazards Earth Syst. Sci.* **2023**, *23*, 361–373. [CrossRef]
39. Yuan, Q.; Wang, G.; Zhu, C.; Lou, D.; Hagan, D.F.T.; Ma, X.; Zhan, M. Coupling of soil moisture and air temperature from multiyear data during 1980–2013 over china. *Atmosphere* **2020**, *11*, 25. [CrossRef]
40. Mao, F.; Cheng, G.; Jin, H. Pergélisol et eau de nappe sur le Plateau Qinghai-Tibet et dans le Nord-Est de la Chine. *Hydrogeol. J.* **2013**, *21*, 5–23. [CrossRef]
41. Li, S.; Jiang, Z.; Zhang, W.; Yu, M. Spatial and temporal variations in precipitation and their influencing factors in China from 1961 to 2010. *Int. J. Climatol.* **2017**, *37*, 345–358. [CrossRef]
42. Huang, Y.; Li, L.; Xu, C.; Cheng, J.; Xu, X.; Zheng, T.; Zhang, X. Spatiotemporal distribution patterns of deadly geohazard events in China, 2013–2019. *Nat. Hazards Res.* **2022**, *2*, 316–324. [CrossRef]
43. Xu, X.; Liu, J.; Zhang, S.; Li, W.; Yan, C.; Wu, S. China's Multi-Period Land Use Land cover Remote sensing Monitoring Dataset (CNLUCC)[EB/OL]. Data Registration and Publishing System of the Resource and Environmental Science Data Center of the Chinese Academy of Sciences 2018. Available online: https://www.resdc.cn/DOI/doi.aspx?DOIid=54 (accessed on 4 January 2023).
44. Chen, J.; Li, R.; Tao, M.; Wang, L.; Lin, C.; Wang, J.; Wang, L.; Wang, Y.; Chen, L. Overview of the performance of satellite fire products in China: Uncertainties and challenges. *Atmos. Environ.* **2022**, *268*, 118838. [CrossRef]
45. Chuvieco, E.; Giglio, L.; Justice, C. Global characterization of fire activity: Toward defining fire regimes from Earth observation data. *Glob. Chang. Biol.* **2008**, *14*, 1488–1502. [CrossRef]